Elsevier Editorial System(tm) for Mechanical Systems and Signal Processing
Manuscript Draft

Manuscript Number:

Title: A method for variable pressure load estimation in spur and helical gear pumps

Article Type: Full Length Article

Keywords: Gear pump; spur gear; helical gear; variable pressure load; dynamic analysis.

Corresponding Author: Dr. Emiliano Mucchi, Ph.D.

Corresponding Author's Institution: University of Ferrara

First Author: Mattia Battarra

Order of Authors: Mattia Battarra; Emiliano Mucchi, Ph.D.

UNIVERSITA' DEGLI STUDI DI FERRARA
DIPARTIMENTO DI INGEGNERIA
Via Saragat, 1 - 44100 FERRARA

Ferrara, 5th of June 2015

A method for variable pressure load estimation in spur and helical gear pumps

By Mattia Battarra, Emiliano Mucchi

Dear Editor,

I'm submitting a paper to be considered for publication.

The paper proposed an original procedure for the analytical determination of variable excitation sources coming from pressure evolution inside tooth spaces in external gear pumps. Pressure force and torque are estimated with respect to the angular position of the gears, taking into account the phenomena that occur during the meshing course. In particular, the paper proposes a general methodology aiming at determining pressure force and torque components along the three coordinates axes and suitable to be applied on both spur and helical gears. The procedure is applied to a tandem gear pump in order to assess its effectiveness with respect to other methods available in the literature. The comparison shows that the present methodology is able to describe a wider range of phenomena involved in the meshing evolution.

Yours sincerely

Emiliano Mucchi

Emiliano MUCCHI, PhD
Assistant Professor
Mechanics of Machines Research Group
EnDIF - Engineering Department in Ferrara
Università degli Studi di Ferrara
Via Saragat, 1
I-44122 Ferrara, Italy
Tel: +39 0532 974913
Mobile: +39 3397661381
Fax: +39 0532 974913
mailto: emiliano.mucchi@unife.it

***Highlights (for review)**

- We propose a novel method for load estimation in gear pumps
- Analytical determination of variable pressure excitation
- The method is assessed via a tandem gear pump dynamic model

A method for variable pressure load estimation in spur and helical gear pumps

M. Battarra, E. Mucchi

Engineering Department, University of Ferrara
Via Saragat, 1 I-44122 Ferrara, Italy

Corresponding Author:
Emiliano Mucchi
Engineering Department, University of Ferrara
Via Saragat, 1 I-44122 Ferrara, Italy
email: emiliano.mucchi@unife.it
tel: +39 0532 974911

ABSTRACT

A systematic procedure is proposed to determine variable excitation sources coming from pressure evolution inside tooth spaces in external gear pumps. Pressure force and torque are estimated with respect to the angular position of the gears, taking into account the phenomena that occur during the meshing course. In particular, the paper proposes a general methodology aiming at determining pressure force and torque components along the three coordinates axes and suitable to be applied on both spur and helical

gears. Firstly, the method to calculate pressure loads acting on a single tooth space during a complete revolution is given, then the total pressure force and torque loading the gear center is obtained. Particular attention is addressed on the description of the helical gear scenario. As an example, the method is applied to a tandem gear pump, characterized by the presence of two stages, one with spur gears and one with helical gears. An experimentally assessed model to analyze the fluid-dynamic behavior of the tandem pump is described and the proposed procedure for pressure load estimation is applied. Eventually, the pressure loads estimated with the present procedure are compared with other estimation methods already described in the literature. The comparison shows that the present methodology is able to describe a wider range of phenomena involved in the meshing evolution.

Keywords

Gear pump, spur gear, helical gear, variable pressure load, dynamic analysis.

1.Introduction

Due to their features regarding the wide operating condition range, small dimensions and costs, spur gear pumps are nowadays considered as useful power sources for several applications (e.g. steering systems, automatic gearboxes and cooling systems). Within this framework, the need to improve their Noise, Vibration and Harshness (NVH) behavior without affecting their performances is becoming more and more compelling. The elasto-dynamic analysis of gear pump is a fundamental task to evaluate the pump's performances in terms of vibrations and emitted noise [1]. As it is well-known, the definition of an effective dynamic model and the load determination generated by the different sources of the pumps are the two main steps to achieve this goal. When modeling the dynamic behavior of a gear pump, a number of main loads has usually to be considered: the torque transmitted by the driving motor, the

meshing forces, the bearing reactions and the torque and force generated by the oil pressure evolution inside tooth spaces [2, 3].

The dynamic behavior of gear-pair systems has been widely studied during the last two decades; several authors have proposed numerical models to take into account periodic meshing stiffness, backlash and the presence of journal bearings [4, 5, 6]. These works took advantages from previous studies focused on the determination of excitation sources, e.g. the periodic meshing stiffness [7] and reactions, e.g. the journal bearing impedance [8, 9]. Moreover, since the improvements in the result quality obtained by these dynamic models are strictly connected with the improvements in the excitation sources and bearing reactions estimation, various methodologies have been later presented. The meshing stiffness has been estimated by means of different approaches, both analytical [10] and numerical [11, 12]. Concurrently, efforts have been given in developing analytical models on journal bearings reaction estimation, based on approximate methods [13, 14] or exact solutions [15].

From this brief review, variable pressure loads result to be the ones with the most critical determination and, thus, with a deep influence on the pump's dynamic behavior and axial balance [16, 17]. A method for pressure force definition is introduced in [16] and later improved in [18], where the loading condition is calculated by a finite difference method and used to analyze the designing of bearing blocks balancing surfaces. The importance related to the determination of pressure force for investigating the performances of external gear pumps was already underlined in [19], being one of the main excitation sources for vibration of the pump case. Nevertheless, in [19] the authors did not provide a systematic method regarding their determination.

Moreover, the need to improve the NVH behavior of gear pumps has led to spread the use of helical gear pumps, mostly where low levels of pressure difference and high flow rates are required, even if, in the literature, this kind of gear pump has been rarely studied. The first works on helical gear pumps date

back to the forties and they were focused on giving some slight details on the instantaneous and mean flow rate [20, 21]. Later, in [22] the author provided an exhaustive explanation on the way the helix affects the theoretical outlet flow ripple. More recently, in [23] the pressure force and torque acting on helical gears has been discussed, nevertheless, the adopted approach is based on simplified hypothesis that led authors to neglect the components due to the presence of the helix, i.e. the axial pressure force and relative torque components.

In the present work, a systematic procedure for the determination of the pressure force and torque acting on the gear shafts is introduced. The purpose is to clearly define an accurate and flexible methodology that can be straightforwardly applied both to simulated and measured pressure data in a wide variety of gear pumps. The outlined method is suitable to analyze both spur and helical gear pumps by determining all the spatial components (forces along three coordinate axes and relative torques). In order to assess this methodology, a tandem pump made of two stages, one with spur gears and one with helical gears, has been studied with a lumped parameter model to determine the tooth space pressure ripple. Hence, the results have been used to evaluate the pressure load by the proposed methodology in comparison with methods already described in the literature.

The contents of the paper are as follows. In Section 2, the original methodology for pressure force and torque estimation is described, focusing the attention on both spur and helical gears. Firstly, the method restricted to spur gears is shown, later it is generalized to helical gears, defining the pressure force along three coordinate axes and the relative torques. Section 3 is devoted to the description of the mechanical standpoint of the tandem pump, taken as an example of application, addressing the mathematical model and relative experimental verification adopted to determine the tooth space pressure ripple for the two stages of the pump. Section 4 concerns the assessment of the methodology for pressure force determination; within this framework, the method, introduced in section two, is applied

on the tandem pump taking advantage of pressure ripple estimated with the lumped parameter model. The results are compared with the ones obtained applying other methods already described in the literature. Eventually, the last section is devoted to concluding remarks.

Nomenclature

β	Helix angle on the pitch circle.
β_B	Oil bulk modulus.
ϑ	Angular position of the reference control volume.
μ	Oil dynamic viscosity.
ρ	Oil density.
ω	Angular speed in rad/s.
A	Surface used to define turbulent flows.
b	Gear width.
C_d	Coefficient of resistance.
F	Pressure force.
$F_{tot,i}$	Total pressure force applied to the gear center by tooth space i.
f_r	Rotational frequency in Hz.
h	Channel height.
i,j	Indexes of the reference control volumes related to the driving gear (*i*) and the driven gear (*j*).
k	Frame of calculus.
L	Channel length.
M	Pressure torque.

$M_{tot,i}$ Total pressure torque applied to the gear center by tooth space i.

n Rotational speed in rpm.

P Oil pressure in the reference control volume.

P_{TANK} Oil pressure inside the tank.

Q_l Volumetric flow rate under laminar condition.

Q_t Volumetric flow rate under turbulent condition.

r,t Subscripts used to indicate the radial (*r*) and tangential (*t*) component of the pressure force applied by a single tooth space.

r_{ext} Radius of the external circle.

r_{root} Radius of the root circle.

u Tangential velocity.

V Volume of the reference control volume.

V_{var} Variable volume added to the inlet/outlet chamber.

w Channel width.

z_n Number of teeth.

x, y, z Superscripts used to indicate the reference Cartesian components of the pressure force and torque.

2.Pressure force and torque estimation

The methodology introduced hereafter can be considered as a complete method to determine the pressure forces and torques in external gear pumps. Figure 1 depicts the reference scheme of the proposed procedure in a generic external gear pump; on the center of each gear, a 3D reference system

is located and the pressure forces applied on the two gears are studied separately. Let consider the generic tooth space V_i of the driving gear and the two adjacent tooth spaces, namely V_j and V_{j-1}, which share oil flow rates during the meshing course. Along a complete revolution, two different configurations are identified, distinguishing if the reference tooth space is outside, or inside, the meshing zone.

2.1.Tooth spaces out of the meshing zone

Within this layout, the oil pressure acts symmetrically on the entire tooth space surface and, therefore, pressure force F_{LR} does not have a tangential component (F_{LR}=$F_{LR,r}$), as it can be seen in Figure 1. In this frame, F_{LR} can be determined, as described in [2], with Eqn. (1):

$$|F_{LR}| = 2 \cdot P_i \cdot \sin\left(\frac{\vartheta_L - \vartheta_R}{2}\right) \cdot b \cdot r_{ext} \quad (1)$$

The absence of a tangential component leads to the absence of pressure torques applied to the gear. The total force loading the gear center can be therefore calculated with Eqns. (2) and (3):

$${F_{tot,i}}^x = -|F_{LR}| \cdot \cos\left(\frac{\vartheta_R + \vartheta_L}{2}\right) \quad (2)$$

$${F_{tot,i}}^y = -|F_{LR}| \cdot \sin\left(\frac{\vartheta_R + \vartheta_L}{2}\right) \quad (3)$$

2.2.Tooth spaces inside the meshing zone

When tooth space V_i enters within the meshing zone, it is necessary to consider that a different discretization of the control volume is adopted and, in particular, three different control volumes

contribute to the definition of the reference tooth space surface (Figure 2.a). It has to be underlined that within such a methodology, the meshing zone starts when the tooth of the driven gear enters into the circle defined by radius r_{ext} and not when the real contact occurs; concurrently, it ends when the tooth of the driven gear exits from the same circle and not when the real contact ends. As a result, the tooth space is divided into three regions, each one under the loading of a different pressure and separated by the contact point *K* and the point of minimum distance *H* (Figure 2). Pressure P_i of the reference control volume acts on the central region, while the two external regions are influenced by pressures P_j and P_{j-1}, belonging to control volumes V_j and V_{j-1} previously defined; the three regions are analyzed separately, defining for each one the acting forces (see Figure 2.b and Figure 2.c).

In the region located on the left side of the tooth space, between points L and K, pressure P_{j-1} is acting and the connected pressure force F_{LK} can be divided in two components along the radial and tangential directions, respectively named $F_{LK,r}$ and $F_{LK,t}$ (Figure 2), calculated with Eqn. (4) and (5):

$$\left|F_{LK,r}\right| = 2 \cdot P_{j-1} \cdot \sin\left(\frac{\vartheta_L - \vartheta_K}{2}\right) \cdot b \cdot r_{ext} \quad (4)$$

$$\left|F_{LK,t}\right| = P_{j-1} \cdot b \cdot (r_{ext} - r_K) \quad (5)$$

The presence of a non-zero tangential component leads to the non-zero pressure torque M_{LK}, which can be calculated with the following equation (6):

$$|M_{LK}| = \left|F_{LK,t}\right| \cdot \left(\frac{r_{ext} + r_K}{2}\right) \quad (6)$$

The force F_{LK} has now to be referred into the coordinates system of Figure 1 using Eqn. (7) and (8):

$$F_{LK}{}^{x} = -\left|F_{LK,r}\right| \cdot \cos\left(\frac{\vartheta_L + \vartheta_K}{2}\right) - \left|F_{LK,t}\right| \cdot \sin\left(\frac{\vartheta_L + \vartheta_K}{2}\right) \quad (7)$$

$$F_{LK}{}^{y} = -\left|F_{LK,r}\right| \cdot \sin\left(\frac{\vartheta_L + \vartheta_K}{2}\right) + \left|F_{LK,t}\right| \cdot \cos\left(\frac{\vartheta_L + \vartheta_K}{2}\right) \quad (8)$$

A similar procedure can be applied to the right side of the tooth space, between points H and R (Figure 2): here pressure P_j produces force F_{HR}, defined along the radial and tangential directions, and torque M_{HR}, which can be calculated with Eqn. (9), (10) and (11):

$$\left|F_{HR,r}\right| = 2 \cdot P_j \cdot \sin\left(\frac{\vartheta_H - \vartheta_R}{2}\right) \cdot b \cdot r_{ext} \quad (9)$$

$$\left|F_{HR,t}\right| = P_j \cdot b \cdot (r_{ext} - r_H) \quad (10)$$

$$|M_{HR}| = \left|F_{HR,t}\right| \cdot \left(\frac{\vartheta_H + \vartheta_R}{2}\right) \quad (11)$$

As done regarding F_{LK}, force F_{HR} has to be referred into the coordinates system in Figure 1 applying Eqn. (12) and (13):

$$F_{HR}{}^{x} = -\left|F_{HR,r}\right| \cdot \cos\left(\frac{\vartheta_H + \vartheta_R}{2}\right) + \left|F_{HR,t}\right| \cdot \sin\left(\frac{\vartheta_H + \vartheta_R}{2}\right) \quad (12)$$

$$F_{HR}{}^{y} = -\left|F_{HR,r}\right| \cdot \sin\left(\frac{\vartheta_H + \vartheta_R}{2}\right) - \left|F_{HR,t}\right| \cdot \cos\left(\frac{\vartheta_H + \vartheta_R}{2}\right) \quad (13)$$

The middle part of the tooth space, which results to be bounded by points K and H, is subjected to pressure P_i; in this case, the pressure force is additionally subdivided into two forces, namely F_{KM} and F_{MH}. Force F_{KM} and torque M_{KM} are determined with Eqn. (14), (15) and (16):

$$\left|F_{KM,r}\right| = 2 \cdot P_i \cdot \sin\left(\frac{\vartheta_K - \vartheta_M}{2}\right) \cdot b \cdot r_{ext} \quad (14)$$

$$\left|F_{KM,t}\right| = P_i \cdot b \cdot (r_K - r_M) \quad (15)$$

$$|M_{KM}| = \left|F_{KM,t}\right| \cdot \left(\frac{\vartheta_K + \vartheta_M}{2}\right) \quad (16)$$

Concurrently, force F_{MH}, and the relative torque M_{MH}, are calculated with Eqn. (17), (18) and (19):

$$\left|F_{MH,r}\right| = 2 \cdot P_i \cdot \sin\left(\frac{\vartheta_M - \vartheta_H}{2}\right) \cdot b \cdot r_{ext} \quad (17)$$

$$\left|F_{MH,t}\right| = P_i \cdot b \cdot (r_H - r_M) \quad (18)$$

$$|M_{MH}| = \left|F_{MH,t}\right| \cdot \left(\frac{r_M + r_H}{2}\right) \quad (19)$$

Focusing the attention on Figure 2.b and Figure 2.c, it can be noticed that the layout of the applied

forces changes during the meshing evolution; in particular, it depends on the position of the contact point with respect to the line of action. When the meshing occurs along the line of approach (Figure 2.b), radius $r_K < r_H$ and $r_K = r_M$; therefore, $F_{KM,t}$ becomes zero, as well as torque M_{KM}, while $F_{MH,t}$ is applied on the right flank of the tooth space. On the opposite, when the meshing occurs along line of recess (Figure 2.c), radius $r_K > r_H$ and $r_H = r_M$; therefore, $F_{MH,t}$ becomes zero, as well as M_{MH}, while $F_{KM,t}$ is applied on the left flank of the tooth space.

Force F_{KH}, defined as the sum of F_{KM} and F_{MH}, is calculated with Eqn. (20) and (21):

$$F_{KH}{}^{x} = -|F_{KM,r}| \cdot \cos\left(\frac{\vartheta_K + \vartheta_M}{2}\right) - |F_{KM,t}| \cdot \sin\left(\frac{\vartheta_K + \vartheta_M}{2}\right) - |F_{MH,r}| \cdot \cos\left(\frac{\vartheta_M + \vartheta_H}{2}\right) + |F_{MH,t}| \cdot \sin\left(\frac{\vartheta_M + \vartheta_H}{2}\right) \quad (20)$$

$$F_{KH}{}^{y} = -|F_{KM,r}| \cdot \sin\left(\frac{\vartheta_K + \vartheta_M}{2}\right) + |F_{KM,t}| \cdot \cos\left(\frac{\vartheta_K + \vartheta_M}{2}\right) - |F_{MH,r}| \cdot \sin\left(\frac{\vartheta_M + \vartheta_H}{2}\right) - |F_{MH,t}| \cdot \cos\left(\frac{\vartheta_K + \vartheta_H}{2}\right) \quad (21)$$

The total force $F_{tot,i}$ and the total torque $M_{tot,i}$ loading the gear center can be obtained from the sum of all the contributions estimated above:

$$F_{tot,i}{}^{x} = F_{LK}{}^{x} + F_{KH}{}^{x} + F_{HR}{}^{x} \quad (22)$$

$$F_{tot,i}{}^{y} = F_{LK}{}^{y} + F_{KH}{}^{y} + F_{HR}{}^{y} \quad (23)$$

$$M_{tot,i} = -|M_{HR}| - |M_{MH}| + |M_{LK}| + |M_{KM}| \quad (24)$$

Once the calculus of the pressure force and torque has been terminated for a complete revolution, it is possible to determine the total loads acting on the gear center as the sum of each tooth space

contribution. Thus, this final step allows the calculation of the variable pressure force (and torque) at each frame of calculus k along the pitch, which is the fundamental period of such loads (Eqn. (25), (26) and (27)).

$$F_{tot}{}^{x}(k) = \sum_{i=1}^{z_n} F_{tot,i}{}^{x}(k) \quad (25)$$

$$F_{tot}{}^{y}(k) = \sum_{i=1}^{z_n} F_{tot,i}{}^{y}(k) \quad (26)$$

$$M_{tot}(k) = \sum_{i=1}^{z_n} M_{tot,i}(k) \quad (27)$$

The present procedure can be straightforwardly applied to the driven gear; in this case if V_j is the reference control volume, then it is necessary to take into account the influence of control volumes V_i and V_{i+1}.

2.3.Model extension to helical gears

Hereafter, the methodology has been extended to helical gears, with the aim to define a general method for pressure force and torque estimation.

In order to estimate pressure force and torque under the effects of helix, the helical gear is divided into an arbitrary number of spur gears, obtained by cutting the helical one along the axial direction. The methodology for calculating the pressure force and torque is applied to each spur gear by using Eqns. (1-

24), obtaining the evolution of such loads along a complete revolution. It has to be underlined that in case of helical gears the oil pressure is acting perpendicularly with respect to the teeth surface. Therefore, to correctly determine the pressure force components along axes x and y, pressure P_i, P_j and P_{j-1} should be multiplied by $\cos(\beta)$.

Moreover, the application of such procedure cannot be considered exhaustive: the particular shape of helical gears necessarily causes the presence of non-zero components of the pressure force along the axial direction, and two more components of the pressure torque, along axes x and y. Hence, it has to be considered that, in case of helical gears, pressure force and torque should be expressed along all the three Cartesian coordinates. Thus, with the aim of defining a general method, the procedure has been extended to all the remaining components.

2.3.1.Helical tooth spaces out of the meshing zone.

Along the axial direction, the tooth space appears to be unbalanced only inside the meshing zone. In this latter case, the calculus of the pressure force along the axial direction depends on the position of the contact point with respect to the line of action, as previously explained about F_{KH}. Within this framework, when the meshing occurs along the line of approach, force ${F_{KM}}^z$ is equal to zero even if the radial component exists; the same effect is obtained regarding ${F_{MH}}^z$ when the meshing occurs along the line of recess. Nevertheless, a single equation can be obtained to determine ${F_{tot,i}}^z$:

$$ {F_{tot,i}}^z = \pm \tan(\beta) \cdot \left(|F_{LK,r}| + |F_{LK,t}| - |F_{HR,r}| - |F_{HR,t}| + |F_{KM,t}| - |F_{MH,t}| + \frac{1 + sign(r_K - r_H)}{2} |F_{KM,r}| - \frac{1 - sign(r_K - r_H)}{2} |F_{MH,r}| \right) \quad (28) $$

The correct choice between plus or minus in Eqn. (28) depends on the type of gears analyzed and, in particular, whether they are right-handed or left-handed gears.

Regarding the estimation of pressure torque along axes x and y, an approach similar to the one proposed for the definition of the pressure torque along axial direction is hereafter defined, but applied to all the positions assumed by the tooth space during a complete revolution. Focusing the attention on a tooth space outside the meshing zone, such a tooth space is not balanced with respect to the torque along axes x and y. Moreover, to calculate its value it is necessary to firstly divide the tooth space in two specular parts, namely right-side and left-side, through his axial plane of symmetry and later determine the pressure force applied on each part along axis z. Thus, Eqn. (29) and (30) show the two opposite forces, which have the same amplitude and a different loading point (Figure 3).

$$F_{LN}{}^{z} = \pm \tan(\beta) \cdot \left({}^{F_{LR}}/_{2} + P_i \cdot b \cdot (r_{ext} - r_{root}) \right) \quad (29)$$

$$F_{NR}{}^{z} = \mp \tan(\beta) \cdot \left({}^{F_{LR}}/_{2} + P_i \cdot b \cdot (r_{ext} - r_{root}) \right) \quad (30)$$

Again, the correct choice between plus or minus depends on the type of gears analyzed. It is now possible to directly calculate the pressure torque along axis x and y using Eqn. (31) and (32).

$$M_{tot,i}{}^{x} = F_{NR}{}^{z} \cdot \left(\frac{r_{ext} + r_{root}}{2} \right) \cdot \cos\left(\vartheta_{M_R}\right) - F_{LN}{}^{z} \cdot \left(\frac{r_{ext} + r_{root}}{2} \right) \cdot \cos\left(\vartheta_{M_L}\right) \quad (31)$$

$$M_{tot,i}{}^{y} = F_{NR}{}^{z} \cdot \left(\frac{r_{ext} + r_{root}}{2} \right) \cdot \sin\left(\vartheta_{M_R}\right) - F_{LN}{}^{z} \cdot \left(\frac{r_{ext} + r_{root}}{2} \right) \cdot \sin\left(\vartheta_{M_L}\right) \quad (32)$$

By assuming that each force, $F_{NR}{}^{z}$ and $F_{LN}{}^{z}$, acts along the axis of symmetry of the angular sector which

defines it, angles ϑ_{M_R} and ϑ_{M_L} are respectively defined by Eqn. (33) and (34):

$$\vartheta_{M_R} = \vartheta_R - \frac{2\pi}{4z_n} \mp \frac{\pi}{2} \quad (33)$$

$$\vartheta_{M_L} = \vartheta_L + \frac{2\pi}{4z_n} \pm \frac{\pi}{2} \quad (34)$$

2.3.2.Helical tooth spaces into the meshing zone.

The same procedure can be applied to tooth spaces inside the meshing zone. In particular, in Figure 2, the tooth space is divided into the two specular parts (right-side causing ${M_{HR}}^{\beta}$, ${M_{NH}}^{\beta}$, and left-side causing ${M_{LK}}^{\beta}$ and ${M_{KN}}^{\beta}$) and their contribution to the pressure torque components along axes x and y is estimated. When the meshing occurs along the line of approach, the pressure torque components caused by the left-side are:

$$\left|{M_{LK}}^{\beta}\right| = \tan(\beta) \cdot \left(\left|F_{LK,r}\right| + \left|F_{LK,t}\right|\right) \cdot \left(\frac{r_{ext} + r_K}{2}\right) \quad (35)$$

$$\left|{M_{KN}}^{\beta}\right| = \tan(\beta) \cdot P_i \cdot b \cdot \left[2 \cdot r_K \cdot \sin\left(\frac{\vartheta_K - \vartheta_N}{2}\right) \cdot \left(\frac{r_{root} + r_K}{2}\right) + \left(\frac{{r_K}^2 - {r_{root}}^2}{2}\right)\right] \quad (36)$$

Concurrently, the pressure torque components caused by the right-side are:

$$\left|{M_{HR}}^{\beta}\right| = \tan(\beta) \cdot \left(\left|F_{HR,r}\right| + \left|F_{HR,t}\right|\right) \cdot \left(\frac{r_{ext} + r_H}{2}\right) \quad (37)$$

$$\left|{M_{NH}}^{\beta}\right| = \tan(\beta) \cdot P_i \cdot b \cdot \left[2 \cdot r_H \cdot \sin\left(\frac{\vartheta_N - \vartheta_H}{2}\right) \cdot \left(\frac{r_{root} + r_H}{2}\right) + \left(\frac{{r_H}^2 - {r_{root}}^2}{2}\right)\right] \quad (38)$$

Therefore, the total pressure torque applied along the Cartesian axes x and y are obtained applying equations (39) and (40), respectively:

$${M_{tot,i}}^{x} = \mp\left|{M_{LK}}^{\beta}\right| \cdot \sin\left(\frac{\vartheta_L + \vartheta_K}{2}\right) \mp \left|{M_{KN}}^{\beta}\right| \cdot \sin\left(\frac{\vartheta_K + \vartheta_N}{2}\right) \pm \left|{M_{NH}}^{\beta}\right| \cdot \sin\left(\frac{\vartheta_N + \vartheta_H}{2}\right) \pm \left|{M_{HR}}^{\beta}\right| \cdot \sin\left(\frac{\vartheta_H + \vartheta_R}{2}\right) \quad (39)$$

$${M_{tot,i}}^{y} = \pm\left|{M_{LK}}^{\beta}\right| \cdot \cos\left(\frac{\vartheta_L + \vartheta_K}{2}\right) \pm \left|{M_{KN}}^{\beta}\right| \cdot \cos\left(\frac{\vartheta_K + \vartheta_N}{2}\right) \mp \left|{M_{NH}}^{\beta}\right| \cdot \cos\left(\frac{\vartheta_N + \vartheta_H}{2}\right) \mp \left|{M_{HR}}^{\beta}\right| \cdot \cos\left(\frac{\vartheta_H + \vartheta_R}{2}\right) \quad (40)$$

Once the calculus has been repeated for every spur gear which the helical gear was divided into, it is necessary to execute a numerical integration along the width of the gear for all the components x, y and z of pressure force $F_{tot,i}$ and torque $M_{tot,i}$. The result is the variation of the actions produced by the oil pressure inside a helical tooth space during a revolution; in order to obtain the total actions applied on the gear center along the angular pitch, Eqn. (25) must be applied and extended to every component of the pressure force and torque.

3. Application: tandem gear pump.

3.1 Mechanical set up

In order to assess the methodology on both spur and helical gears, the procedure has been applied on a tandem gear pump, which is described in detail in the present section. The tooth space pressure

ripple has been firstly calculated applying a numerical model, later the results have been validated, in terms of outlet pressure ripple and volumetric efficiency, with experimental data, hence the pressure force and torque have been determined.

Generally, a tandem pump consists of two couples of coaxial gearwheels. The tandem pump being studied has one gear stage working at high pressure level and the other stage working at a lower pressure level. The two driver gears and the two driven gears are located on the same driving and driven shafts, respectively, being the stages coaxial. This mechanical setup forces the stages to work at the same mean angular velocity. Figure 4 shows the setup of the pump: the Low-Pressure Stage, hereafter called LPS, is located directly inside the casing and consists of two helical gearwheels with same number of teeth. The LPS is hydraulically divided from the High-Pressure Stage, namely HPS, by a mid-plate. The HPS consists of a couple of external spur gearwheels, which work between the mid-plate and the cover-plate. Two couples of journal bearings, directly shaped inside the casing and the cover-plate, support the rotating shafts. The HPS and LPS share a common inlet chamber, whilst they have two separated outlet chambers. The LPS and HPS are put in communication with inlet and their relative outlet chambers by the presence of grooves that allow the oil to flow inside and outside the tooth spaces easily. At the same time, grooves are shaped in order to keep the chambers hydraulically divided by the pressurization zone and the meshing zone, where the relief grooves.

The clearance between the shafts and the mid-plate holes is rather large; thus, a slight friction between them is present. In this scenario, the two volumes defined between the shaft and the mid-plate can be considered such as “drainage chambers” that slightly connect the two stages and allow oil exchange.

3.2 .Variable pressure modeling

A brief review of the mathematical approach used to determine the pressure variation around the gear pump for a complete gear rotation is given, focusing the attention on the control volumes scheme adopted to model the tandem pump and the several flow rates determined for each stage. The complexity of the pump geometry, due to the presence of the double stage, several grooves and the LPS with helical gears, has led to develop a lumped parameter (LP) model which uses some results provided by a Computational Fluid Dynamic (CFD) model. The LP approach has been adopted to evaluate the performances of the tandem pump in terms of outlet mass flow rate, outlet pressure ripple, oil pressure evolution for both the LPS and HPS during a complete gear rotation and instantaneous volumetric efficiency. Concurrently, in order to improve the LP model results accuracy, a 2D and a 3D CFD model have been developed. These models have been used with the aim at investigating some specific fluid dynamics phenomena that occur in several pump areas that play an important role in the resulting oil pressure. The complete CFD model will be presented in further papers of the authors.

Regarding the LP model, the entire pump and the relative outlet piping system of the test bench have been discretized with a constant number of control volumes in which all the fluid properties are considered as constant. Several authors [2, 24, 25, 26] have already applied a similar approach, each of them proposing a different subdivision of the pump volumes, in particular in the meshing zone. In the present model, the discretization of the meshing zone proposed by Vacca et al. in [24] has been implemented, but a different physical approach has been followed. Assuming that the pump works at constant angular speed, the time dependence of the physical properties can be replaced with an angular dependence and Eqn. (41) can be used to describe the pressure evolution inside each control volume.

$$\frac{dP_i}{d\vartheta} = \frac{\beta_B}{V_i}\left[\frac{1}{\omega}\left(\sum Q_i^{in} - \sum Q_i^{out}\right) - \left(\frac{dV_i}{d\vartheta} - \frac{dV_i^{var}}{d\vartheta}\right)\right] \quad (41)$$

Applying Eqn. (41) to each control volume, with the appropriate definition of the exchanged flows, the unknown pressure can be calculated. Two different categories of flow rates are considered: laminar flow rates and turbulent flow rates. The formers have been defined using the modified Poiseuille's equation (Eqn. (42)), which accounts the dependence from the pressure drop and the contribute of the drag flow:

$$Q_l = \frac{wh^3}{12\mu}\frac{\Delta P}{L} + \frac{whu}{2} \quad (42)$$

The latter have been defined using Eqn. (43), obtained applying the Bernoulli's equation under specific hypotheses:

$$Q_t = C_d A\sqrt{\frac{2|\Delta P|}{\rho}}sign(\Delta P) \quad (43)$$

According to the different links between flow and pressure drop defined by Eqn. (42) and (43), it is important to correctly interpret the nature of the several flows describing the interconnections between volumes.

The tandem pump has been discretized using 65 control volumes: 34 related to the high-pressure gears, 22 to the low-pressure gears, 3 related to the common inlet chamber and the two outlet chambers, 2 to the interconnecting volumes between stages and, finally, 4 to describe the outlet piping system of the

test bench. Figure 5 provides a global view of the model structure and the connections between control volumes. As it can be observed, the 66th control volume, namely TANK, has been added to represent the environmental boundary conditions: the oil pressure inside this volume is not calculated but defined as a constant and equal to the atmospheric pressure. The set of volumetric flow rates that connects the TANK to the inlet chamber and the outlet chamber to the TANK has been considered as turbulent and, therefore, modelled by using Eqn. (43). The turbulent behavior was also used to model the presence of the two valves that define the pressure drop between the outlet pressures (LPS and HPS) and the TANK pressure. The model has been implemented in Matlab environment. In Table 1 the main parameters concerning the physical properties of the oil, considered as constant values, are shown. By using the parameters in Table 1, a mean outlet pressure equal to 30bar for the HPS and 3bar for the LPS and a constant angular step $\Delta\vartheta$ equal to 0.2406°, the time computational cost to simulate a complete rotation is about 4 hours.

3.3.Experimental model verification

In the present subsection the most remarkable results, calculated with the numerical model formerly described, are introduced and discussed, comparing them with some experimental data. A test rig is used to evaluate the tandem pump performances in terms of outlet pressure ripple and outlet mass flow rate. It consists of a common tank, which provides the necessary oil flow rate, and two outlet pipelines, each one connecting the outlet chamber of one stage with the tank. An electrical motor controlled by inverter drives the pump. The outlet pressure provided by the two stages is settled separately on both pipelines through a control valve. A specific system is also used to control and maintain the oil temperature as constant. A high frequency piezoelectric transducer (model PCB S102B) has been used in order to measure the pressure ripple in the pipelines.

Figure 6 shows the comparison between measured and simulated results concerning the outlet

pressure ripple of the LPS (divided by the mean delivery pressure) in time domain during a complete revolution. These results have been obtained considering the pump working at nominal conditions, therefore the initial transient is not taken into account. As it can be noticed, the pressure ripple is characterized by the presence of 11 main peaks, which represent the 11 meshing events occurring along the complete revolution. A similar analysis has been simultaneously conduced for the HPS and the comparison between measured and simulated delivery pressure ripple in time domain is shown in Figure 7. As observed in the LPS results, the outlet pressure ripple is mainly characterized by the presence of a number of peaks equals to the number of meshing events that occur during a complete revolution.

From this analysis, it can be affirmed that the numerical model provides a satisfactory reproduction of the main characteristics of the measured outlet pressure ripple; a good agreement is also obtained comparing the measured and simulated volumetric efficiency of the two stages (see Table 2).

4.Results and discussion

In the present section the results concerning the methodology presented in Section 2 are shown and discussed, comparing them with the results obtained applying previous methods described in [2, 17].

In particular, the pressure evolution in the HPS and LPS estimate din Section 3 has been used as input data for the estimation of the pressure loads by using the proposed methodology (Section 2) and a method proposed in [2], namely past model 1 (PM1), and the method described in [17], namely past model 2 (PM2). These three methods are identified by a different way of modelling the pressure force and torque inside the meshing zone. In particular, in the PM1 the meshing phenomenon is not considered, therefore the pressure force is estimated by using Eqn. (1) along the entire revolution. Moreover, in the PM1 the pressure torque is calculated without considering the effects of the pressure in the tooth space

located between meshing teeth. In the PM2, the effects produced during the meshing evolution on the pressure force are evaluated, but a different definition of the control volumes is used. The PM2 takes into account the effects of the meshing phenomenon just when a double contact point exists. When a single contact point exists, in the PM2 the pressure torque is estimated as in PM1. Moreover, both PM1 and PM2 are explicitly built up to study spur gears and they can be applied on helical gears just under specific hypothesis [23].

Figure 8 shows the comparison between pressure force and torque on both driving and driven gear, obtained by applying the new methodology, namely current methodology CM, and the PM1 for the HPS. The forces (torques) are normalized with respect to the absolute value of the mean pressure force (torque) applied in x (z) direction on the driving gear by using the CM. As already discussed, the PM1 does not take into account the meshing phenomena, which results in a low level of agreement between these two methods. In particular, the estimation of the pressure torque on the driving gear appears to give completely different results (Figure 8.c), while there is, in general, a good accordance regarding the estimation of the pressure torque applied on the driven gear (Figure 8.f). The lack of agreement in the estimation of the pressure torque is due to the different approach: in the CM the pressure torque directly derives from the estimation of the pressure force applied along the tangential direction whilst in the PM1 the pressure torque is evaluated analyzing geometrically the meshing phenomenon.

In order to better understand why the estimation of the pressure force by using PM1 method gives so different results, it is possible to focus the attention, as an example, on the pressure force transmitted along the axis y by the tooth space defined by volume V_j (belonging to the driven gear) during a complete revolution. In Figure 9 the evolution of such pressure force component during a complete revolution calculated by using the CM and by using the PM1 is shown, together with the pressure evolution inside the control volumes used for their determination. As expected, the two forces coincide for the entire

revolution, except for the meshing interval, in which the PM1 does not take into account the effect produced by two phenomena: (i) the light difference between the pressure evolution in control volumes V_j and V_i, and (ii) the pressure drop in control volume V_{i+1} that occurs an angular pitch before the pressure drop in V_i. This latter phenomenon strongly affects the pressure force effectively transmitted to the gear axis and, therefore, it cannot be neglected. The phenomenon (ii), in particular, is taken into account in the calculus procedure defined by PM2, which has been demonstrated to give more accurate results with respect to PM1 in the elasto-dynamic analysis of gear pumps [17].

Figure 10 shows the same comparison between the CM and the PM2 in the HPS. As it can be noticed, the two methods provide an almost coincident estimation of the pressure force transmitted along x direction, while a major level of discordance is observed in the estimation of the pressure force transmitted along y direction. These light discrepancies occur because of the procedure defined in PM2, which does not take into account the phenomenon (i). The oil pressure inside the tooth spaces referred to two meshing teeth, as observed in Figure 9, is almost equal during the meshing evolution. Nevertheless, when these tooth spaces start facing to the inlet chamber, the pressure drop in both control volumes determines an increase of the pressure difference between them and, therefore, a light difference in the pressure force estimated by the two models occurs.

Regarding the pressure torque, it is possible to observe that similar results are obtained only till the 35% of the angular pitch (Figure 10.c and Figure 10.f); the remaining 65% is characterized by a higher level of discordance, especially for the pressure torque applied on the driving gear. The reason of these results has to be found in the modelling procedure defined by PM2, in which the calculus is split in two sub-cases. When there are two pairs of teeth in contact (till about 40% of the angular pitch), the pressure torque estimation takes into account the oil pressure in the control volume between the two pairs of teeth. Therefore, within this angular interval, the pressure torque estimation is similar for both the PM2 and the

CM and the results show a satisfactory agreement. When there is only a pair of teeth in contact, PM2 coincides with PM1, ergo the results show the same differences noticed in Figure 8.

Following this discussion, it can be affirmed that the estimation of the pressure force and torque transmitted by the oil to the gears is strongly influenced by the several phenomena that occur during the meshing interval. By neglecting one of them affects the results with a relevance which depends on the angular extension of the neglected phenomenon itself.

In Figure 11 the results regarding the pressure force (torque) provided by the application of the CM on the helical driving gear located in the LPS are shown as percent of the absolute value of the mean pressure force (torque) along axis x (z).

Focusing the attention on the pressure force along the three axes, it can be noticed that F_Z has a considerable lower magnitude compared to F_X and F_Y. The pressure force along the axial direction strongly depends on the helix angle, which is around 10° for the analyzed gears. Moreover, this aspect becomes even more effective considering the pressure torque along axes x and y, which results to have a magnitude more than 100 times lower than along the axial direction. For this reason, the x and y components of the pressure torque could be neglected for the development of a simplified elasto-dynamic analysis of helical gear pumps. Nevertheless, they could become considerably high in case of high values of outlet pressure and important in order to study the pump balancing or its dynamic behavior.

5.Concluding remarks

This paper presents an analytical methodology for the calculation of pressure forces and torques in both spur and helical gear pumps. The methodology consists in a systematic and general procedure to consider the major number of phenomena, which characterize the meshing evolution. In order to assess

its effectiveness, the methodology has been applied to a real tandem gear pump by comparisons with other methodologies available in the literature.

The comparison has shown that the determination of pressure force and torque transmitted to the gears is strongly influenced by a number of phenomena, which are taken into consideration by the proposed model.

The methodology applied to the helical gear stage enable to estimate all the force and torque components. The obtained results have shown that the pressure force along the axial direction, depending on the helix angle which is usually around 10° in gear pumps, is characterized by a magnitude 10 times lower than the magnitude of the pressure force along the other two directions. Moreover, the shape of helical gears leads to the presence of non-zero components of the pressure torque along axes x and y, even if the magnitude of these components is considerably lower than the pressure torque applied in axial direction. Nevertheless, they could become considerably high in case of high values of outlet pressure and important in order to study the pump balancing or the dynamic behavior in a 3D scenario.

The application of the proposed allows to estimate the real importance of the force components related to the helix and consequently, to evaluate the negligible components with respect to the degree of accuracy needed. The proposed methodology can represent a useful tool to precisely estimate one of the main excitation sources that contribute to define the dynamic behavior of these machines.

Acknowledgment

The authors wish to thank TRW Automotive Italia S.r.l.— Automotive Pumps Division (Ostellato, Ferrara, Italy) and the engineers of this Company for co-operation and assistance in the collection of model data. This work has been developed within the Advanced Mechanics Laboratory (MechLav) of Ferrara

Technopole, realized through the contribution of Regione Emilia-Romagna – Assessorato Attività Produttive, Sviluppo Economico, Piano telematico – POR-FESR2007-2013, Attività I.1.1.

6.References

1. Mucchi E, Rivola A and Dalpiaz G. Modelling dynamic behavior and noise generation in gears pumps: procedure and validation. *Appl Acoust* 2013; 77:99-111.
2. Mucchi E, Dalpiaz G and Fernàndez del Rincòn A. Elastodynamic analysis of a gear pump. part I: pressure distribution and gear eccentricity. *Mech Syst Signal Pr* 2010; 24(7):2160-2179.
3. Mucchi E, Dalpiaz G and Rivola A. Elastodynamic analysis of a gear pump. part II: meshing phenomena and simulation results. *Mech Syst Signal Pr* 2010; 24(7):2180-2197.
4. Arakere N G and Nataraj C. Numerical simulation of nonlinear spur gear dynamics. In: ASME Design Engineering Technical Conferences, Las Vegas, Nevada, USA, 1999.
5. Theodossiades S and Natsiavas S. Non-linear dynamics of gear-pair systems with periodic stiffness and backlash. Journal of Sound and Vibration 2000; 229(2):287-310.
6. Theodossiades S and Natsiavas S. On geared rotordynamic systems with oil journal bearings. Journal of Sound and Vibration 2001; 243(4):721-745.
7. Kahraman A and Singh R. Interactions between time-varying mesh stiffness and clearance nonlinearities in a geared system. Journal of Sound and Vibration 1991; 146:135-156.
8. Childs D, Moes H and Van Leeuwen H. Journal bearing impedance descriptions for rotordynamic applications. ASME Journal of Lubrication Technology 1977; 99:198-210.

9. Van de Vorst E L B, Fey R H B, De Kraker A et al. Steady-state behavior of flexible rotordynamic systems with oil journal bearings. Nonlinear Dynamics 1996; 11:295-313.

10. Kuang H and Yang T. An estimate of mesh stiffness and load sharing ratio of a spur gear pair. In: International Power Transmission and Gear Conference, 1992; pp. 1–9

11. Fernandez del Rincon A, Viadero F, Iglesias M. et al. A model for the study of meshing stiffness in spur gear transmissions. Mechanism and Machine Theory 2013; 61:30-58.

12. Chang L, Liu G and Wu L. A robust model for determining the mesh stiffness of cylindrical gears. Mechanism and Machine Theory 2015; 87:93-114.

13. Bastani Y and De Queiroz M. A new analytic approximation for the hydrodynamic forces in finite-length journal bearings. ASME Journal of Tribology 2010; 132:1-9.

14. Lahmar M, Haddad A and Nicolas D. An optimized short bearing theory for nonlinear dynamic analysis of turbulent journal bearings. Eur. J. Mech. A/Solids 2000; 19:151–177

15. Chasalevris A and Sfyris D. Evaluation of the finite journal bearing characteristics, using the exact analytical solution of the Reynolds equation. Tribology International 2013; 57:216-234.

16. Borghi M, Milani M and Toderi G. Sul calcolo della spinta sulle fiancate nelle machine oleodinamiche ad ingranaggi esterni. In: *51st ATI Congress*, Udine, Italy, 1996 pp. 1675-1687.

17. Mucchi E, Dalpiaz G and Fernàndez del Rincòn A. Elasto-dynamic analysis of a gear pump. part IV: improvement in the pressure ripple distribution modelling. *Mech Syst Signal Pr* 2015; 50-51:193-213.

18. Borghi M, Milani M, Paltrinieri F et al. Studying the axial balance of external gear pumps- SAE paper 2005-01-3634, 2005.

19. Bidhendi M, Foster K and Taylor R. Computer prediction of cyclic excitation sources for an external gear pump. *Journal of Engineering Manufacture* 1985; 199(3):175-180.

20. Meldahl A. Théorie des pompes a engrenages. *Revue Brown Boveri* 1939; pp. 259-261.

21. Takahashi Y. On the trapping of fluid between the teeth of the involute gear pump. *Trans. of the Japan Society of Mechanical Engineers* 1940; 3(6):6-10.

22. Bonacini C. Sulle pompe ad ingranaggi a dentatura elicoidale. *Tecnica Italian* 1965; 3:5-11.

23. Mucchi E and Dalpiaz G. Elasto-dynamic analysis of a gear pump. part III: experimental validation procedure and model extension to helical gears. *Mech Syst Signal Pr* 2015; 50-51:174-192

24. Vacca A and Guidetti M. Modelling and experimental validation of external spur gear machines for fluid power applications. *Simul Model Pract Th* 2011; 19:2007-2031.

25. Falfari S and Pelloni P. Setup of a 1D model for simulating dynamic behaviour of external gear pumps. SAE paper 2007-01-4228, 2007.

26. Mancò S, Nervegna N, Simulation of an external gear pump and experimental verification. In: *1st JHPS International Symposium on Fluid Power,* Tokio, Japan, 1989 pp. 139-152.

TABLES

Table 1. Main parameters used to determine the pressure distribution.

Parameters	Value
β_B	$1.13 \cdot 10^9$ Pa
μ	0.0103 Pa·s
ρ	806.7 kg/m^3
P_{TANK}	10^5 Pa
n	3020 rpm

Table 2. Comparison between calculated and measured volumetric efficiency.

Stage	Simulated efficiency	Measured efficiency
LPS	0.980	0.987
HPS	0.787	0.890

FIGURES

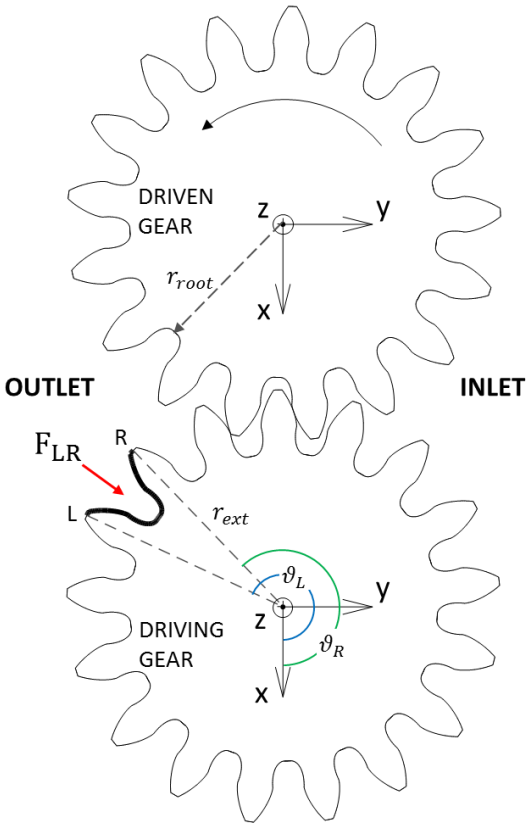

Figure 1. Reference scheme for pressure force determination.

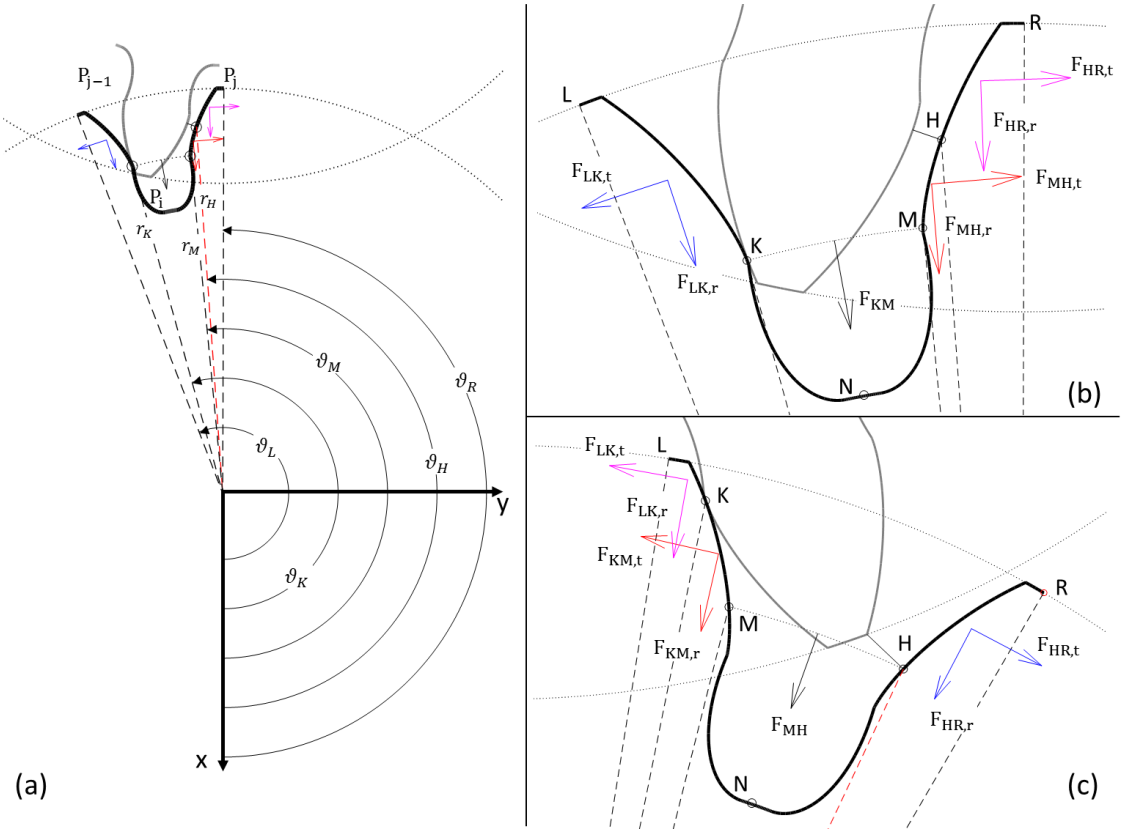

Figure 2. Discretization of the tooth space in the meshing zone (a), and definition of the forces loading the tooth space surface in detail, along the line of approach (b) and along the line of recess (c).

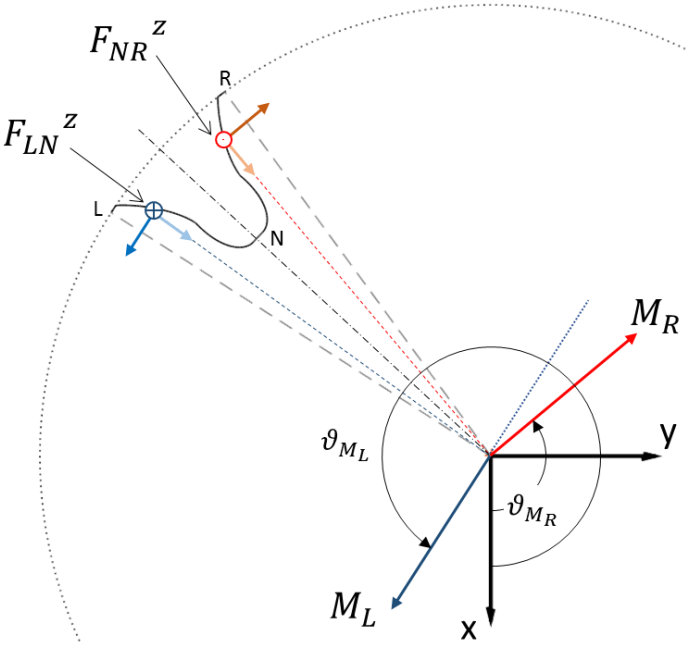

Figure 3. Pressure torque modelling when the tooth space is outside the meshing zone.

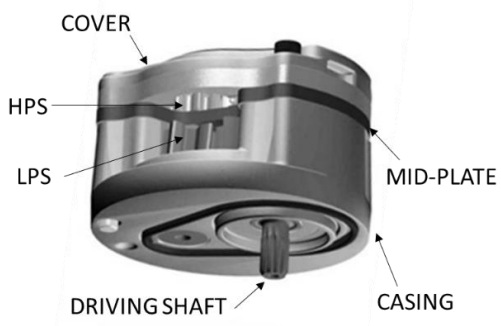

Figure 4. Mechanical setup of the tandem pump.

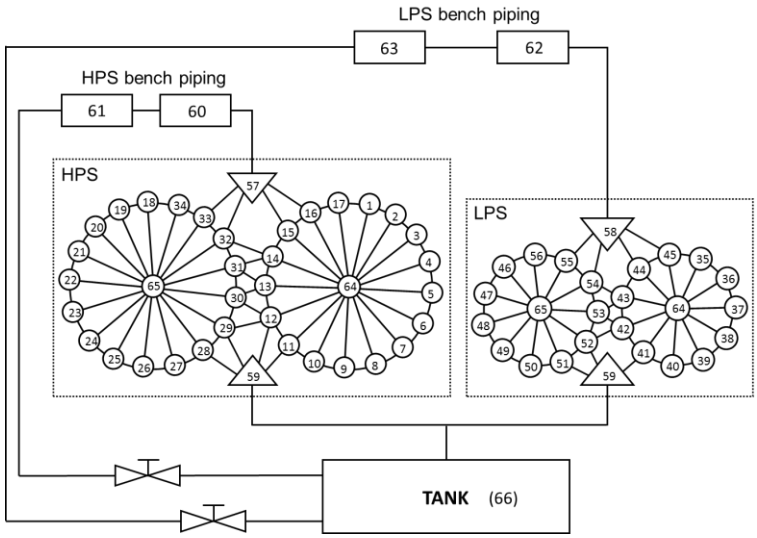

Figure 5. Control volumes and relative connections.

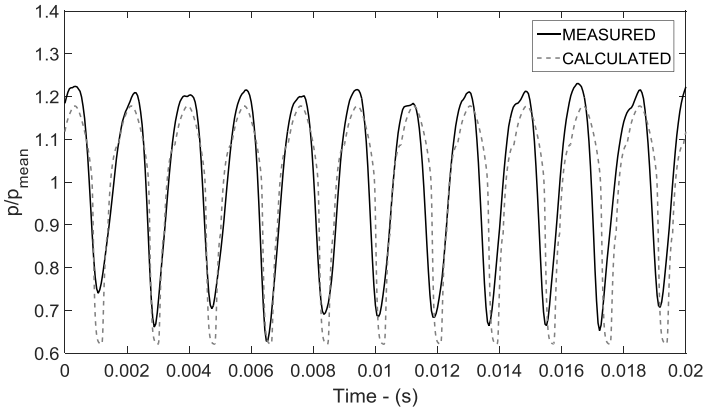

Figure 6. Comparison between measured and calculated outlet pressure of the LPS.

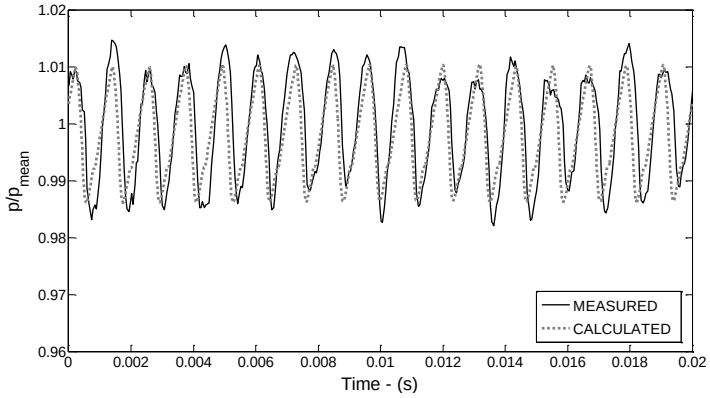

Figure 7. Comparison between measured and calculated outlet pressure of the HPS.

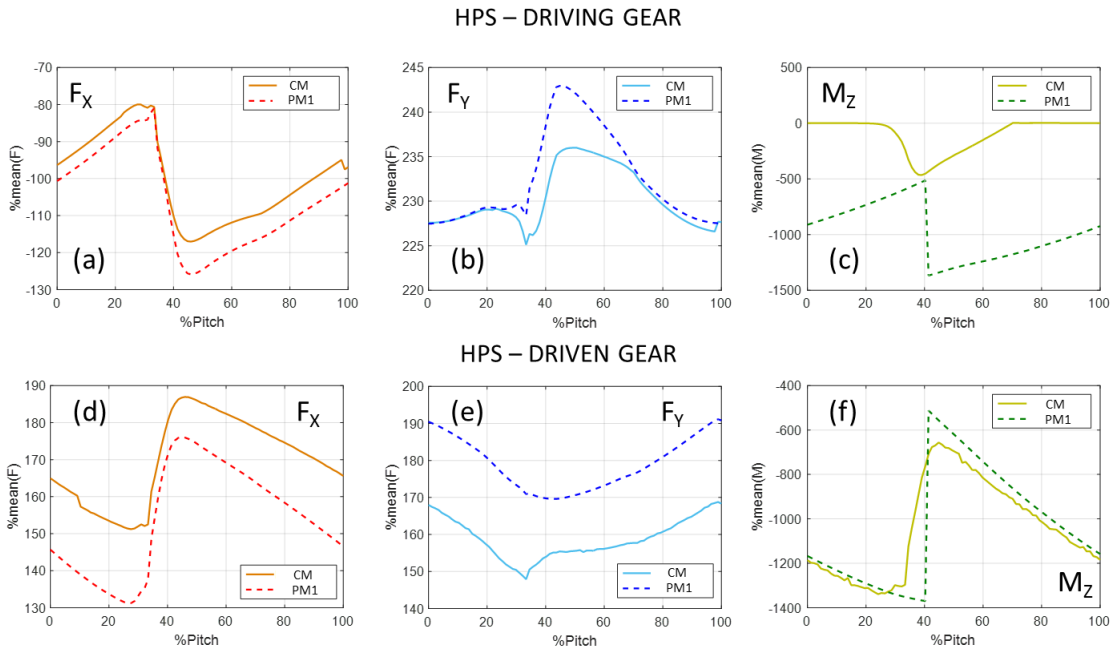

Figure 8. Comparison between pressure force and torque along the angular pitch for both driving and driven gear, in the HPS, calculated with the PM1 and the CM.

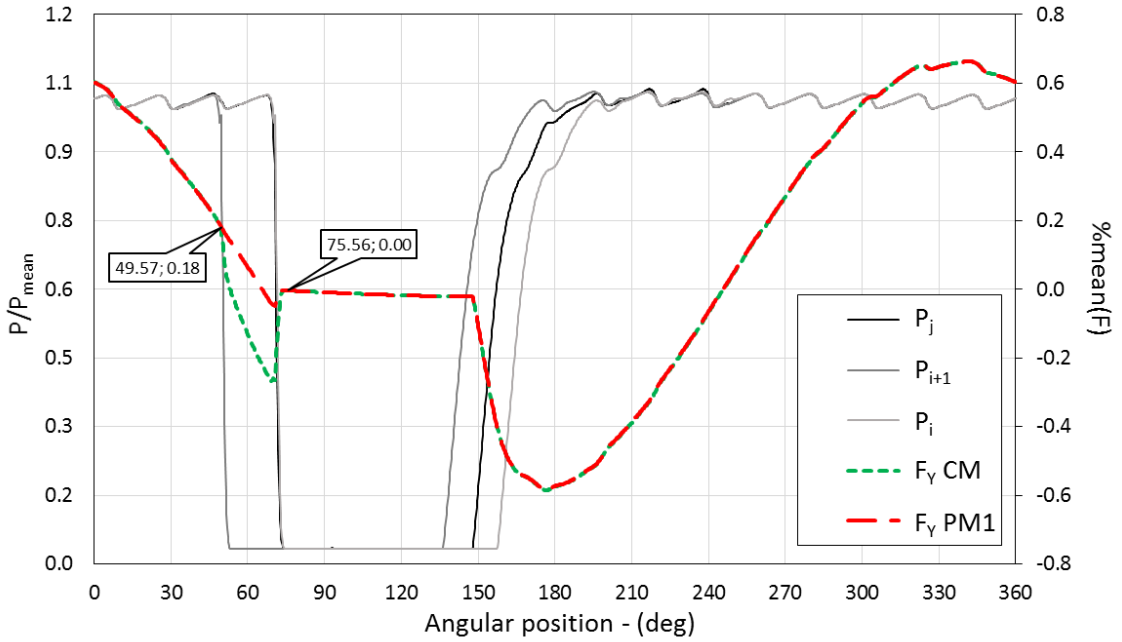

Figure 9. F_Y transmitted by a single tooth space V_j during a complete revolution estimated by using the CM and by using the PM1; pressure evolution in the tooth spaces used for the force estimation.

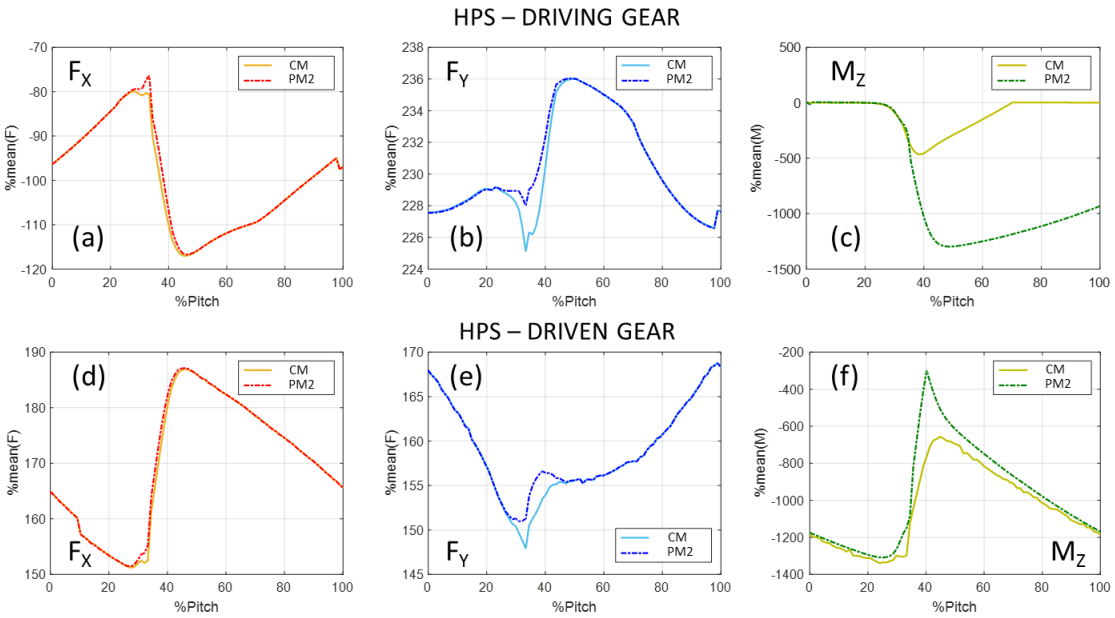

Figure 10. Comparison between pressure force and torque along the angular pitch for both driving and driven gear, in the HPS, calculated with the PM2 and the CM.

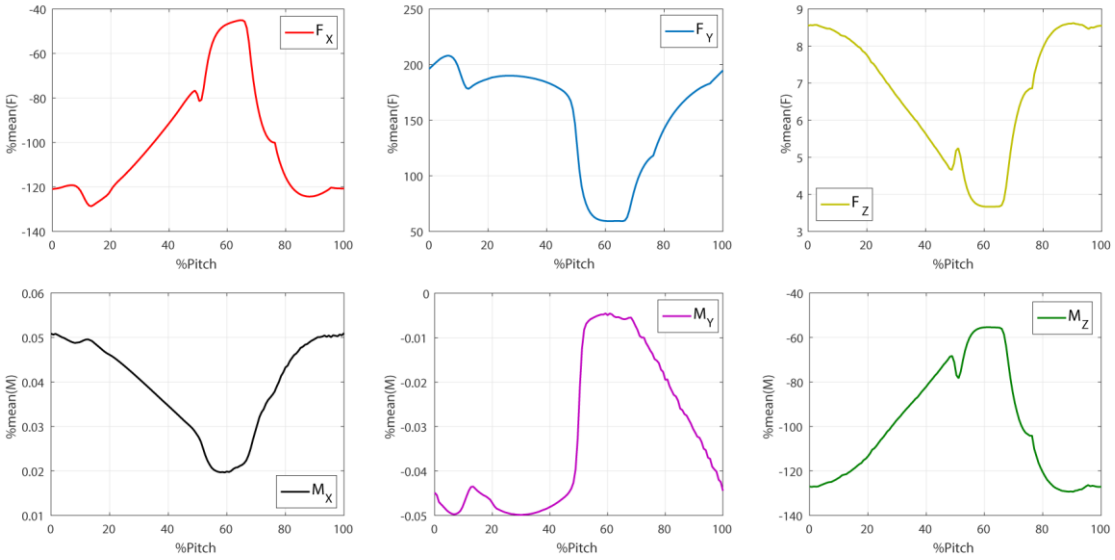

Figure 11. Pressure force and torque applied on the driving gear of the LPS.